

Numerical Simulation of Turbulent Heat Transfer and Fluid Flow in Different Tube Designs

Taiwo O. Oni and Manosh C. Paul

Abstract— Numerical simulation was carried out to study the heat transfer, friction factor and thermal performance of water inside different tubes induced with different twisted tapes. The purpose is to ascertain which of the tube designs gives the best performance when compared with the plain tube. The tubes were under uniform wall heat flux condition and Reynolds number in the range $5000 \leq Re \leq 20000$ were considered. RNG $\kappa - \varepsilon$ equation model was selected for the numerical simulations and RANS equations were employed to render the Navier-Stokes equations tractable. The best performance was obtained when the tube was fitted with alternate-axis triangular cut twisted tape. Its Nusselt number and friction factor are respectively 2.07 – 3.33 and 10.65 – 13.1 times better than that of a plain tube and its thermal performance factor is 1.35 – 1.43 times better than that of the tube with plain twisted tape.

Index Terms—performance, heat transfer, numerical simulation, turbulent flow, twisted tape

I. INTRODUCTION

THE need for improvement in performance of heat transfer equipment has led to the analyses of its heat transfer and fluid flow characteristics. Numerical techniques have made several contributions to such analyses. Chiu and Jang [1] carried out numerical and experimental analyses for thermal-hydraulic characteristics of air flow inside a circular tube with longitudinal strip inserts and found out that of all the different tape inserts used to improve the heat transfer, that of the twisted tape produced the highest improvement, being 13-61% higher than those of plain tubes. However, their analyses did not include what the heat transfer would be if cuts were made on the tape insert that produced the highest improvement.

Eiamsa-ard et al [2] numerically predicted the effects of clearance ratio and twisted ratio in a circular tube induced with twisted tape inserts. The simulation was conducted in the turbulent regime for the Reynolds number ranging from 3000 to 10000. There were no cuts on the tape and hence the

effect which the cuts on a tape will have on the heat transfer was not analysed.

Other works [3-6], among others, have been carried out with the aim of ascertaining improvement in heat transfer and fluid flow in a tube induced with modified twisted tape inserts. There has not been a report on numerical simulation of heat transfer and fluid flow for tube designs induced with twisted tape insert with emphasis on cuts with different geometrical shapes but equal area. This shall be looked into in this work.

II. DESCRIPTION OF COMPUTATIONAL DOMAIN

The domains consist of tubes induced individually with different twisted tape. The tube has dimensions of length 1000mm and diameter 19mm; the twisted tape inserts has a width of 18mm, thickness of 1mm and axial length of 1000mm. The different twisted tape inserts used for the domain are shown in Fig. 1. The three different geometrical shapes chosen as the cuts on the tapes are ellipse, circle, and triangle. These cuts have different geometrical shapes but the same area; that is, they are different-shape-equal-area cuts. The different computational domains used are plain tube (PT), tube with plain twisted tape (TPT), tube with elliptical cut twisted tape (TECT), tube with circular cut twisted tape (TCCT), tube with triangular cut twisted tape (TTCT), tube with alternate-axis elliptical cut twisted tape (TAECT), tube with alternate-axis circular cut twisted tape (TACCT) and tube with alternate-axis triangular cut twisted tape (TATCT).

III. MATHEMATICAL ANALYSIS

The finite volume approach is employed to solve the governing partial differential equations. The tubes were under uniform wall heat flux condition and the inlet water temperature was specified as 301K. Reynolds number in the range $5000 \leq Re \leq 20000$ were considered. The working fluid is considered to be incompressible and the flow is assumed to be steady-state.

The thermal properties (density, ρ ; specific heat capacity, C_p ; Prandtl number, Pr ; thermal conductivity, k and kinematic viscosity, ν) of water for $278K \leq T_f \leq 363K$ as provided by [7] are given in (1) - (5).

Manuscript received March 13, 2014; revised March 30, 2014.

This work was supported by Tertiary Education Trust Fund Nigeria and Ekiti State University Ado-Ekiti Nigeria.

T. O. Oni is with the Systems, Power & Energy Research Division, School of Engineering, University of Glasgow, Glasgow G12 8QQ (e-mail: t.oni.1@research.gla.ac.uk).

M. C. Paul is with the Systems, Power & Energy Research Division, School of Engineering, University of Glasgow, Glasgow G12 8QQ (corresponding author. Tel.: +44(0)141 330 8466, Fax: +44(0)141 330 8466, e-mail: Manosh.Paul@glasgow.ac.uk).

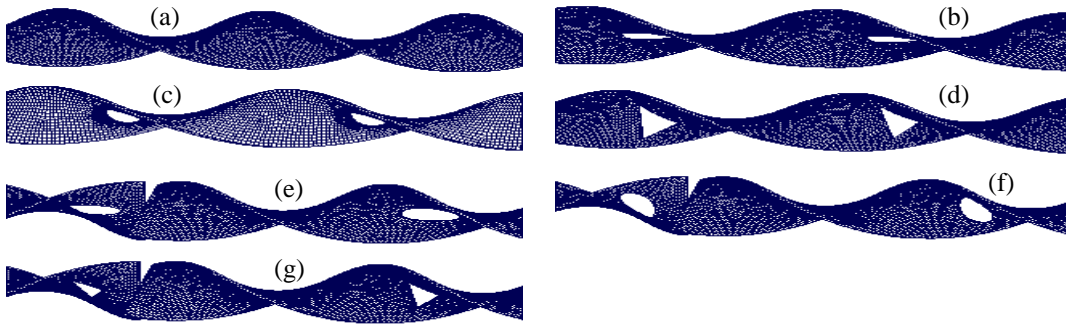


Fig. 1. Twisted tape inserts: (a) plain twisted tape, (b) elliptical cut twisted tape, (c) circular cut twisted tape, (d) triangular cut twisted tape, (e) alternate-axis elliptical cut twisted tape, (f) alternate-axis circular cut twisted tape, (g) alternate-axis triangular cut twisted tape.

$$\rho = 330.116 + 5.91516T_f - 1.631041$$

$$X 10^{-2}T_f^2 + 1.3323 X 10^{-5}T_f^3$$

$$C_p = (10.01128 - 5.135 X 10^{-2}T_f + 1.492117$$

$$X 10^{-4}T_f^2 - 1.4278X 10^{-7}T_f^3) X 10^3$$

$$Pr = 899.99 - 7.78920T_f + 2.2641337$$

$$X 10^{-2}T_f^2 - 2.204026 X 10^{-5}T_f^3$$

$$k = -12.15974 + 0.1181916T_f - 3.6632142$$

$$X 10^{-4}T_f^2 + 3.8084136 X 10^{-7}T_f^3$$

$$\nu = 1.083828 X 10^{-4} - 9.330538 X 10^{-7}T_f$$

$$+ 2.7027447 X 10^{-9}T_f^2 - 2.6243211 X 10^{-12}T_f^3$$

A. Navier-Stokes Equations

The heat transfer and fluid flow were modelled by using the Navier-Stokes governing equations for incompressible flow. They are continuity, momentum and energy equations [8, 9].

(a) Continuity equation:

$$\nabla \cdot \mathbf{V} = 0 \quad (6)$$

(b) Momentum equation:

$$\rho \frac{\partial \mathbf{V}}{\partial t} + \nabla \cdot (\rho \mathbf{V} \mathbf{V}) = -\nabla p + \nabla \cdot \mu (\nabla \mathbf{V}) \quad (7)$$

(c) Energy equation:

$$\rho c_p \left(\frac{\partial T}{\partial t} + \nabla \cdot \mathbf{V} T \right) = \nabla \cdot (k \nabla T) \quad (8)$$

where μ is the dynamic viscosity, p is the pressure, T is the temperature, \mathbf{V} is the velocity vector, and C_p is the heat capacity at constant pressure.

B. Reynolds-Averaged Navier-Stokes Equations

Reynolds Averaged Navier-Stokes (RANS) equations are employed to render the Navier-Stokes equations tractable so that the small-scale turbulent fluctuations do not have to be directly simulated. The approach introduces additional unknown variables in the governing equations. The additional unknown variables are determined by turbulence models.

The RANS equation for mass conservation can be written

$$(1) \quad \text{in the form in tensor form as} \quad \frac{\partial}{\partial x_i} (\rho u_i) = 0 \quad (9)$$

(2) The momentum equation for the time-averaged Navier-Stokes equation is given in tensor form as

$$\rho \frac{D \bar{u}_i}{Dt} = S_i - \frac{\partial \bar{p}}{\partial x_i} + \frac{\partial}{\partial x_j} \left(\mu \frac{\partial u_i}{\partial x_j} - \rho \overline{u'_i u'_j} \right) \quad (10)$$

(3) By employing Boussinesq equation [8, 10], the term $-\rho \overline{u'_i u'_j}$ is written as

$$(4) \quad -\overline{u'_i u'_j} = \nu_t \left(\frac{\partial u_i}{\partial x_j} + \frac{\partial u_j}{\partial x_i} \right) - \frac{2}{3} k \delta_{ij} \quad (11)$$

The time-averaged energy equation is written as

$$(5) \quad \frac{\partial}{\partial x_j} \rho c_p (u_j T) = u_j \frac{\partial p}{\partial x_j} + u'_j \frac{\partial p'}{\partial x_j} + \frac{\partial}{\partial x_j} \left(k \frac{\partial T}{\partial x_j} - \rho c_p \overline{u'_j T'} \right) \quad (12)$$

C. Standard κ - ε model

The standard κ - ε model is a two-equation turbulence model proposed by [11]. The two terms on which the model is based are the turbulent kinetic energy (κ) and dissipation rate of turbulence kinetic energy (ε).

The transport equations, turbulent viscosity (μ_t) and model constants for the standard κ - ε models are given below [9]:

$$(7) \quad \frac{\partial}{\partial t} (\rho \kappa) + \frac{\partial}{\partial x_i} (\rho \kappa u_i) = \frac{\partial}{\partial x_j} \left[\left(\mu + \frac{\mu_t}{\sigma_\kappa} \right) \frac{\partial \kappa}{\partial x_j} \right] + G_\kappa + G_b - \rho \varepsilon - Y_M + S_\kappa \quad (13)$$

$$(8) \quad \frac{\partial}{\partial t} (\rho \varepsilon) + \frac{\partial}{\partial x_i} (\rho \varepsilon u_i) = \frac{\partial}{\partial x_j} \left[\left(\mu + \frac{\mu_t}{\sigma_\varepsilon} \right) \frac{\partial \varepsilon}{\partial x_j} \right] + C_{1\varepsilon} \frac{\varepsilon}{\kappa} (G_\kappa + C_{3\varepsilon} G_b) - C_{2\varepsilon} \rho \frac{\varepsilon^2}{\kappa} + S_\varepsilon \quad (14)$$

$$\mu_t = \rho C_\mu \frac{\kappa^2}{\varepsilon} \quad (15)$$

where G_κ is the generation of turbulence kinetic energy due to the mean velocity gradients; G_ε is the generation of turbulence kinetic energy due to buoyancy; Y_M represents the contribution of the fluctuation to the overall dissipation rate; $C_{1\varepsilon}$, $C_{2\varepsilon}$, $C_{3\varepsilon}$ are model constants; the quantities σ_κ and σ_ε are the turbulent Prandtl numbers for κ and ε respectively; S_κ and S_ε are user-defined source terms. The

model constants are $C_{1\varepsilon} = 1.44$, $C_{2\varepsilon} = 1.92$, $C_\mu = 0.09$, $\sigma_\kappa = 1.0$ and $\sigma_\varepsilon = 1.3$ [9].

D. RNG $\kappa - \varepsilon$ model

Renormalization Group theory (RNG) $\kappa - \varepsilon$ model is a two-equation model proposed by [12] and is based on model transport equations for the turbulence kinetic energy (κ) and its dissipation rate (ε). It improves the accuracy of flows by the reason of an additional term in its transport equation for turbulence dissipation rate (ε).

The transport equations and turbulent viscosity for the RNG $\kappa - \varepsilon$ models are given below [9]:

$$\frac{\partial}{\partial t}(\rho\kappa) + \frac{\partial}{\partial x_i}(\rho\kappa u_i) = \frac{\partial}{\partial x_j} \left[\alpha_\kappa \mu_{eff} \frac{\partial \kappa}{\partial x_j} \right] + G_\kappa + G_b - \rho\varepsilon - Y_M + S_\kappa \quad (16)$$

$$\frac{\partial}{\partial t}(\rho\varepsilon) + \frac{\partial}{\partial x_i}(\rho\varepsilon u_i) = \frac{\partial}{\partial x_j} \left[\alpha_\varepsilon \mu_{eff} \frac{\partial \varepsilon}{\partial x_j} \right] + C_{1\varepsilon} \frac{\varepsilon}{\kappa} (G_\kappa + C_{3\varepsilon} G_b) - C_{2\varepsilon} \rho \frac{\varepsilon^2}{\kappa} - R_\varepsilon + S_\varepsilon \quad (17)$$

where α_κ and α_ε are the inverse effective Prandtl numbers for κ and ε respectively; $C_{1\varepsilon} = 1.42$, $C_{2\varepsilon} = 1.68$, $C_\mu = 0.0845$, $\sigma_\kappa = 0.7194$ and $\sigma_\varepsilon = 0.7194$ are model constants [9].

IV. NUMERICAL TECHNIQUES

The finite volume method is used to discretise the governing partial differential equations encountered in this work. The equations of motion are integrated over a control volume, meaning that momentum and mass are conserved locally within it and also in the calculation domain. The discretisation is carried out with second order upwind scheme by which the unknown quantities at the cell faces are computed through a Taylor series expansion of the cell centered solution about the cell centroid [13]. As a way of incorporating the effects of pressure into the solution for the momentum equation, the SIMPLE (Semi Implicit Pressure Linked Equations) algorithm was used to couple the calculations of pressure and velocity [8, 14]. Fluent 6.3 [9] is used to obtain iterative solution of these equations.

A. Grid Generation

In order to confirm accuracy of the numerical solutions, grid independence tests were conducted for the domains. Six grids with different cells were used for each domain as given in Table I. In selecting the appropriate grid for the simulation, consideration was given to solution precision as well as convergent time. The grid resolution study reveal that PT, TPT, TECT, TCCT, TTCT, TAECT, TACCT and TATCT become independent of the grid at cells 512420, 1015216, 1247298, 1349142, 1374099, 1651206, 1730639 and 2515756 cells respectively. Therefore, these grids were adopted for the domains.

B. Validation with standard $\kappa - \varepsilon$ model and RNG $\kappa - \varepsilon$ model

The Nusselt number obtained with the standard $\kappa - \varepsilon$ and RNG $\kappa - \varepsilon$ turbulence models for PT and TPT were

validated with experimental results and established correlations. The objective is to ascertain the model which gives results that are closer to the experimental data and hence to know which of the models to be selected to perform other numerical simulations. Nusselt number for PT were validated with the result of Seemawute and Eiamsa-ard experiment [15] and correlation of Gnielinski [16]. For TPT, the validations were carried out with the result of Seemawute and Eiamsa-ard experiment [15], Kidd's correlation [17] and Drizius et. al correlation [18].

The validation results, depicted in Fig. 2, reveal that the Nusselt numbers for PT are in agreement with the Seemawute and Eiamsa-ard experimental results and the Gnielinski correlation within deviation of $\pm 5.23\%$ and $\pm 7.67\%$ respectively for the standard $\kappa - \varepsilon$ model as against $\pm 3.02\%$ and $\pm 6.25\%$ respectively for the RNG $\kappa - \varepsilon$ model. It is seen in Fig. 3 that Nusselt numbers agree with the experimental data within $\pm 5.44\%$ and with the Kidd correlation and Drizius et. al correlation within $\pm 6.09\%$ and 7.16% respectively for the standard $\kappa - \varepsilon$ model as against $\pm 3.89\%$, $\pm 5.28\%$ and 7.2% respectively for the RNG $\kappa - \varepsilon$ model. On the overall, the RNG $\kappa - \varepsilon$ model is more accurate and reliable than the standard $\kappa - \varepsilon$ model and is therefore selected for other numerical simulations in this work.

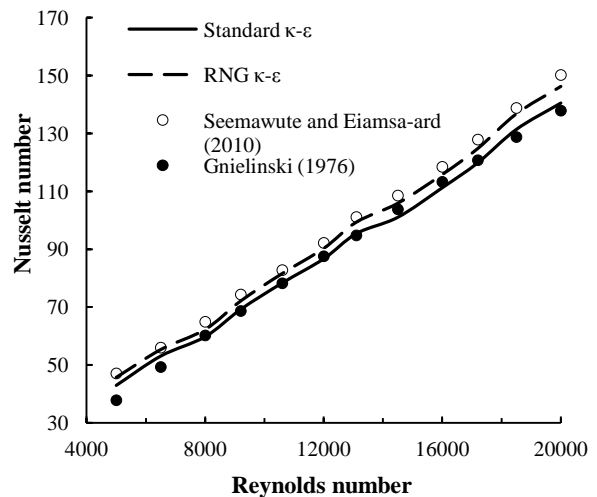


Fig. 2. Validation with standard $\kappa - \varepsilon$ and RNG $\kappa - \varepsilon$ turbulence models for PT.

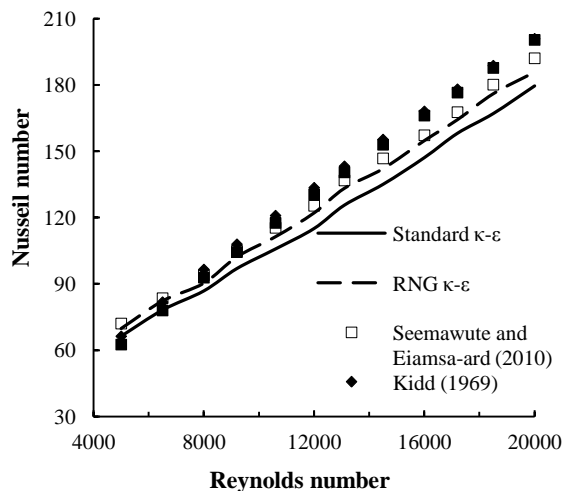


Fig. 3. Validation with standard $\kappa - \varepsilon$ and RNG $\kappa - \varepsilon$ turbulence models for TPT.

TABLE I
GRID RESOLUTION STUDY

Domain		Grid Cell				
PT	461178	476554	512420	614904	717388	768630
TPT	913594	944154	1015216	1218259	1421302	1522824
TECT	1122468	1159966	1247298	1496758	1746217	1870947
TCCT	1214178	1254681	1349142	1618970	1888799	2023713
TTCT	1236639	1277931	1374099	1648919	1923739	2061149
TAECT	1486055	1535641	1651206	1981447	2311688	2476809
TACCT	1557545	1609513	1730639	2076767	2422895	2595959
TATCT	1255502	1658638	2515756	3018907	3522058	3773634

V. COMPUTATIONAL RESULTS AND DISCUSSIONS

A. Flow Field

The velocity vectors at an axial location of 0.866m for all the tubes are shown in **Fig. 4**. The tangential velocity in the plain tube (frame a) is almost zero and therefore makes the swirl near the wall to disappear and weaken the swirl in the entire area. When the plain tube is induced with tape insert the tangential velocity increases and swirl flow is generated around the tapes (frame b, c, d and e). When the tapes are modified by alternating their axes (frame f, g and h), the tangential velocity becomes higher and the swirl becomes stronger than when there are no cuts on the tape inserts. Thus the pattern of the swirl differs from one tube to another as a result of the different types of tape inserts in the tubes.

B. Temperature Contour

The contours of temperature for the length of the twisted tape inserts for the turbulent flow are shown below in **Fig. 5**. When the PT is induced with a plain twisted tape (frame b), the thermal boundary layer grows thinner. In addition, the temperature gradient becomes larger. Thus, the temperature distribution in TPT (frame b) is better than that of PT (frame a). With the replacement of the plain twisted tape with twisted tape with cuts (frames c, d and e), the boundary layer thickness is further reduced and more swirls are generated. These result in better temperature distribution. The tubes induced with tapes with alternate axes (frames f, g and h) have better mixing than those without alternate axes. Consequently, the temperature distribution in TACCT, TATCT and TAECT are better than those in TECT, TCCT and TTCT.

C. Turbulent Kinetic Energy

The influence of tape inserts on the turbulent kinetic energy can be seen in **Fig. 6**. The turbulent kinetic energy in each of the tube designs has its highest value near the wall. With the exception of TCCT and TATCT, it has its least value near the centre of the cross-section. It should be noted that it increases when a tape insert is introduced into PT. As a result of swirl having more strength in tubes induced with tape insert with cuts, the turbulent kinetic energy in TECT, TCCT and TTCT are higher than that of PT. It increases further when the tubes are induced with alternate axes with cuts.

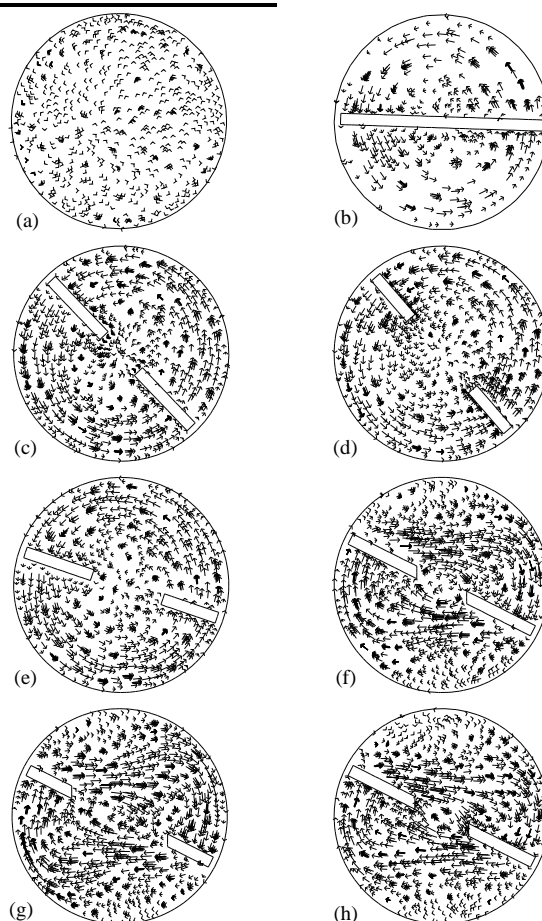


Fig. 4. Velocity vector across tube cross-section at axial location 0.866m for $Re=20000$ for different tubes: (a) PT, (b) TPT, (c) TECT, (d) TCCT, (e) TTCT, (f) TAECT, (g) TACCT, (h) TATCT.

D. Heat Transfer

The effect of the various twisted tape on heat transfer is presented in **Fig. 7**. The Nusselt numbers of the induced tubes are higher than those of the PT. This is as a result of increase of the tangential velocity and decrease of the flow cross-sectional area of the induced tubes which cause the fluid inside them swirls with a higher velocity. The Nusselt number of TPT is 1.26 – 1.52 times better than that of PT. The Nusselt number of TECT, TCCT and TTCT are respectively 1.38 – 1.83, 1.35 – 1.65 and 1.41 – 1.91 times better than that of PT. For TAECT, TACCT and TATCT, their Nusselt numbers are respectively 2.04 – 3.19, 2.00 – 3.07 and 2.07 – 3.33 times better than that of PT. The Nusselt number of tubes with alternate-axes twisted tape is higher than those with twisted tape whose axes do not

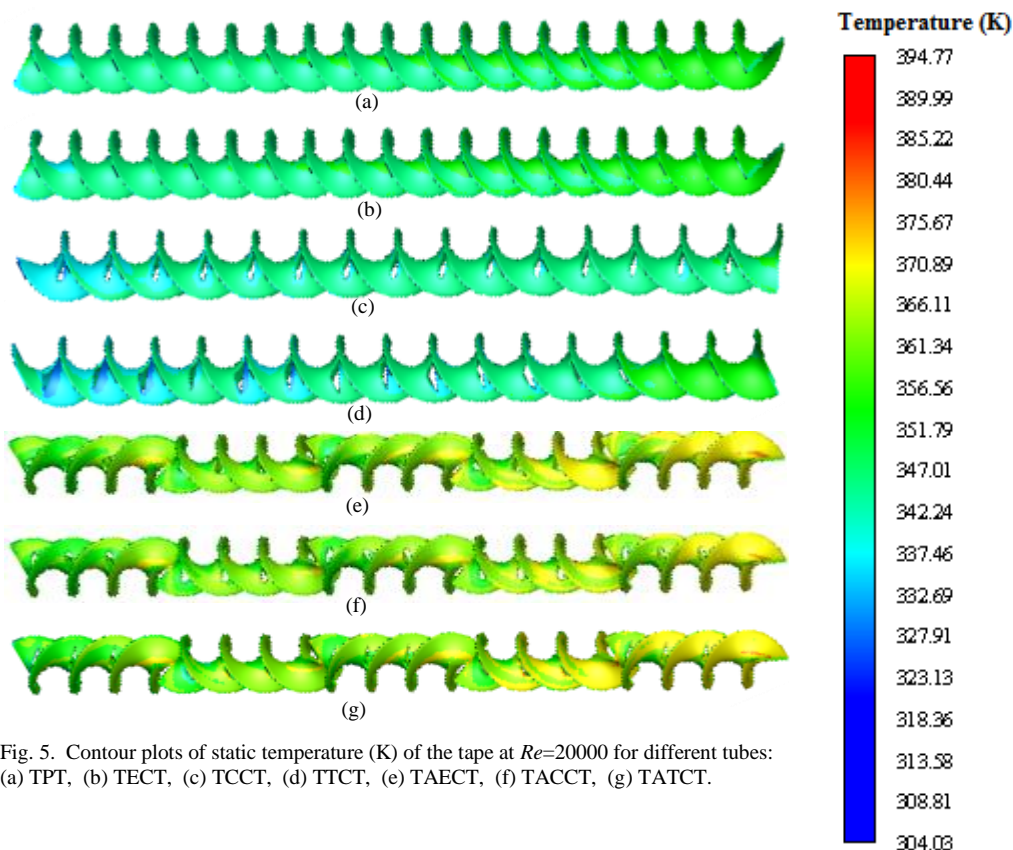


Fig. 5. Contour plots of static temperature (K) of the tape at $Re=20000$ for different tubes: (a) TPT, (b) TECT, (c) TCCT, (d) TTCT, (e) TAECT, (f) TACCT, (g) TATCT.

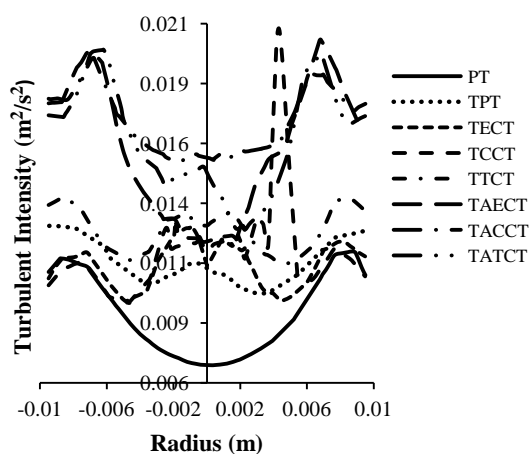


Fig. 6. Turbulent kinetic energy (m^2/s^2) across tube cross-section at axial location 0.866m for $Re=20000$ for different tubes: (a) PT, (b) TPT, (c) TECT, (d) TCCT, (e) TTCT, (f) TAECT, (g) TACCT, (h) TATCT.

alternate. This is due to better fluid mixing near a tube wall caused by the alternate points. Thus, the highest Nusselt number occurs in TATCT.

E. Friction Factor

Fig. 8 illustrates the variation of the friction factor with Reynolds number for the different tube design. The falling trend is sharper as any of the twisted tape is placed inside the tube in comparison with the PT. Of all the induced tapes, TPT has the lowest friction factor. This is caused by the decrease of the blocking effect at the insert wall as well as decrease of the swirling flow. The friction factor of TPT is 4.08 – 4.15 over that of the PT. For the same reason

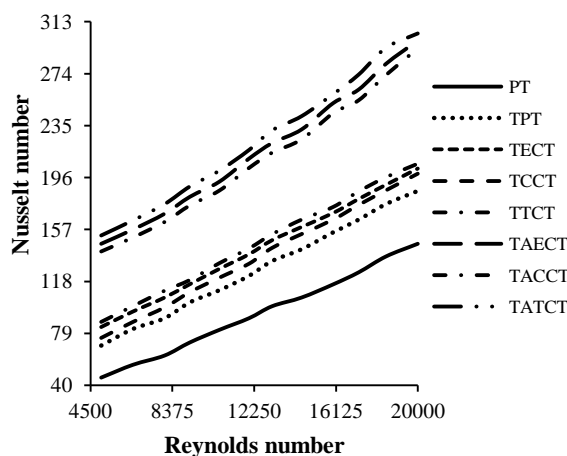


Fig. 7. Effect of different twisted tape on Nusselt number vs. Reynolds number.

presented for the TPT, the friction factor of the TCCT is lower compared with the TECT. The friction factor in TECT, TCCT and TTCT are respectively 4.53 – 4.59, 4.42 – 4.50 and 4.62 – 4.76 over that of the PT. For the TAECT, TACCT and TATCT, their friction factors are respectively 10.29 – 12.66, 10.05 – 12.37 and 10.65 – 13.11 over that of the PT.

F. Thermal Performance Factor

The thermal performance factor (η) is a measure of the possibility of a twisted tape for practical applications in enhancement of heat transfer [19-21]. It is mathematically defined as

$$\eta = \frac{Nu/Nu_p}{(f/f_p)^{1/3}} \quad (18)$$

where Nu and Nu_p are the Nusselt number of the induced tube and plain tube respectively while f and f_p are friction factor of the induced tube and plain tube respectively. The variation of the thermal performance factor for the different tube designs are compared in **Fig. 9**. It shows that the highest values are produced by TATCT while the PT has the lowest performance among the other tube designs. The thermal performance factor of TECT, TCCT and TTCT are respectively 1.22 – 1.25, 1.14 – 1.23 and 1.24 – 1.27 times that of TPT. For TAECT, TACCT and TATCT, their thermal performance factor are respectively 1.30 – 1.38, 1.26 – 1.32 and 1.35 – 1.43 times that of TPT.

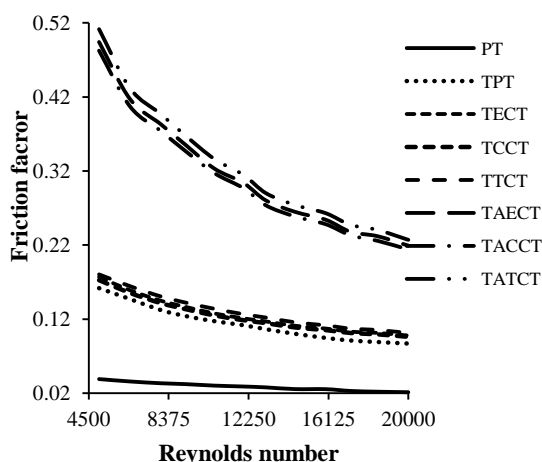


Fig. 8. Effect of different twisted tape on friction factor vs. Reynolds number.

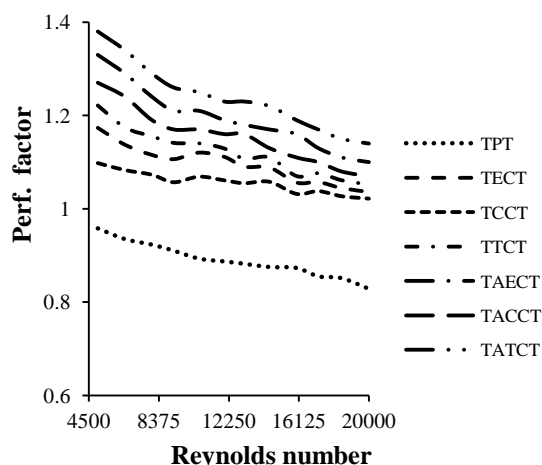


Fig. 9. Effect of different twisted tape on thermal performance factor vs. Reynolds number.

REFERENCES

[1] Y. Chiu and J. Jang, "3D numerical and experimental analysis for thermal-hydraulic characteristics of air flow inside a circular tube with different tube inserts," *Appl. Therm. Eng.*, vol. 29, pp. 250-258, 2009.

[2] S. Eiamsa-ard, K. Wongcharee, and S. Sripattanapipat, "3-D numerical simulation of swirling flow and convective heat transfer in a circular tube induced by means of loose-fit twisted tapes," *Int. Comm. Heat and Mass Transfer*, vol. 36, pp. 947-955, 2009.

[3] P. Murugesan, K. Mayilsamy, S. Suresh, and P. S. S. Srinivansan, "Heat transfer and pressure drop characteristics of turbulent flow in a tube fitted with trapezoidal-cut twisted tape insert," *Int. J. Acad. Res.*, vol. 1, pp. 123-128, Sept. 2009.

[4] P. Murugesan, K. Mayilsamy, and S. Suresh, "Turbulent heat transfer and pressure drop in a tube fitted with square-cut twisted tape," *J. Chem. Eng. Chinese*, vol. 18, no. 4, pp. 609-617, Jul. 2010.

[5] S. W. Chang, Y. J. Jan, and J. S. Liou, "Turbulent heat transfer and pressure drop in tube fitted with serrated twisted tape," *Int. J. Therm. Sci.*, vol. 46, pp. 506-518, Jul. 2007.

[6] T. Cui and M. Tian, "Three-dimensional numerical simulation of thermalhydraulic performance of a circular tube with edgefold-twisted-tape inserts," *J. Hydrodynamics*, vol. 22, no. 5, pp. 662-670, Jul. 2010.

[7] W. M. Kays and M. E. Crawford, *Convection heat and mass transfer*. 2nd ed. McGrawHill Companies, 1980.

[8] H. K. Versteeg and W. Malalasekera, *An introduction to computational fluid dynamics- the finite volume method*. 2nd ed. England: Pearson, 2007.

[9] FLUENT 6.3 User's Guide, Fluent Inc., 2006.

[10] J. O. Hinze, *Turbulence* New York: McGraw-Hill Publishing Co, 1975.

[11] B. E. Launder and D. B. Spalding, *Lectures notes in mathematical models of turbulence* London: Academic Press, 1972.

[12] V. Yakhot and S. A. Orszag, "Renormalization group analysis of turbulence I: Basic theory," *J. Scientific Computing*, vol. 1, no. 1, pp. 1-51, 1986.

[13] C. T. Shaw, *Using computational fluid dynamics* UK: Prentice Hall International Ltd., 1992.

[14] S. V. Patankar and D. B. Spalding, "A calculation procedure for heat, mass and momentum transfer in three- dimensional parabolic flows," *Int. J. Heat Mass Transfer*, vol. 15, pp. 1787-1806, 1972.

[15] P. Seemawute and S. Eiamsa-Ard, "Thermohydraulics of turbulent flow through a round tube by peripherally-cut twisted tape with an alternate axis," *Int. Comm. Heat and Mass Transfer*, vol. 37, pp. 652-659, 2010.

[16] V. Gnielinski, "New equations for heat and mass transfer in turbulent pipe and channel flow," *Int. J. Chem. Eng.*, vol. 16, pp. 359-368, 1976.

[17] G. J. Kidd, "Heat transfer and pressure drop for nitrogen flowing in tubes containing twisted tapes," *J. AIChE*, vol. 15, pp. 581-585, 1969.

[18] M. R. Drizius, R. K. Shkema, and A. A. Shlanciauskas, "Heat transfer in a twisted stream of water in a tube," *Int. Chem. Eng.*, vol. 20, pp. 486-489, 1980.

[19] Q. Liao and M. D. Xin, "Augmentation of convective heat transfer inside tubes with three-dimensional internal extended surfaces and twisted-tape inserts," *Chem. Eng. J.*, vol. 78, pp. 95-105, 2000.

[20] M. A. Akhavan-Behabadi, R. Kumar, A. Mohammadpour, and M. Jamali-Asthiani, "Effect of twisted tape insert on heat transfer and pressure drop in horizontal evaporators for the flow of R-134a," *Int. J. Ref.*, vol. 32, pp. 922-930, 2009.

[21] K. Wongcharee and S. Eiamsa-ard, "Friction and heat transfer characteristics of laminar swirl flow through the round tubes inserted with alternate clockwise and counter-clockwise twisted-tapes," *Int. Comm. Heat and Mass Transfer*, vol. 38, pp. 348-352, 2011.